amirf

NASA TECHNICAL NOTE

NASA TN D-7480

NASA TN D-7480

ZERO-GRAVITY VENTING OF THREE REFRIGERANTS

by Thomas L. Labus, John C. Aydelott, and Geraldine E. Amling

Lewis Research Center
Cleveland, Ohio 44135

NATIONAL AERONAUTICS AND SPACE ADMINISTRATION • WASHINGTON, D. C. • JANUARY 1974

1. Report No.	2. Government Accession No.	3. Recipient's Catalog No.
NASA TN D-7480		

4. Title and Subtitle	5. Report Date
ZERO-GRAVITY VENTING OF THREE REFRIGERANTS	January 1974
	6. Performing Organization Code
7. Author(s)	8. Performing Organization Report No.
Thomas L. Labus, John C. Aydelott, and Geraldine E. Amling	E-7509
	10. Work Unit No.
9. Performing Organization Name and Address Lewis Research Center National Aeronautics and Space Administration Cleveland, Ohio 44135	909-72
	11. Contract or Grant No.
	13. Type of Report and Period Covered
12. Sponsoring Agency Name and Address National Aeronautics and Space Administration Washington, D. C. 20546	Technical Note
	14. Sponsoring Agency Code

15. Supplementary Notes

16. Abstract

An experimental investigation of venting cylindrical containers partially filled with initially saturated liquids under zero-gravity conditions was conducted in the NASA Lewis Research Center 5-second zero-gravity facility. The effect of interfacial mass transfer on the ullage pressure response during venting was analytically determined, based on a conduction analysis applied to an infinitely planer (flat) liquid-vapor interface. This pressure response was compared with both the experimental results and an adiabatic decompression computation.

17. Key Words (Suggested by Author(s))		18. Distribution Statement
Mass transfer	Weightlessness	Unclassified - unlimited
Refrigerants	Venting	

19. Security Classif. (of this report)	20. Security Classif. (of this page)	21. No. of Pages	22. Price*
Unclassified	Unclassified	~~40~~ 42	Domestic, $3.00 Foreign, $5.50

* For sale by the National Technical Information Service, Springfield, Virginia 22151

ZERO-GRAVITY VENTING OF THREE REFRIGERANTS

by Thomas L. Labus, John C. Aydelott, and Geraldine E. Amling

Lewis Research Center

SUMMARY

An experimental investigation of venting cylindrical containers partially filled with initially saturated liquids under zero-gravity conditions was conducted in the NASA Lewis Research Center 5-second zero-gravity facility. The test fluids possessed a near 0° contact angle on the cylindrical container surface resulting in a hemispherical liquid-vapor interface shape in zero gravity. The effect of interfacial mass transfer on the ullage pressure response during venting was analytically determined. This pressure response was compared with both the experimental pressure response and the pressure response based on an adiabatic decompression computation. The results showed that interfacial mass transfer, based on a conduction analysis applied to an infinitely planer (flat) liquid-vapor interface, in a lumped system analysis is significant in determining the ullage pressure response. The pressure response computations from adiabatic decompression consistently yielded too large a predicted ullage pressure decrease. Inclusion of the interfacial mass transfer effects resulted in approximately a 30-percent improvement in the predicted pressure response.

INTRODUCTION

The use of high-energy liquid propellants in our space program has led to a need for information concerning the thermodynamic behavior of cryogenic fluids in tanks which are vented or depressurized in space. The task of venting in low gravity has been successfully accomplished during a number of past missions with venting systems that rely exclusively on auxiliary thrusters to actively position the liquid propellant away from the tank vent.

Short-term venting has been employed by the Saturn S-IV-B (ref. 1) and the Centaur (ref. 2) vehicles in near-Earth orbit. The methods of pressure control include using the vented propellant vapor to provide adequate acceleration to keep the liquid propellant settled at the end of the tank opposite the vent or using auxiliary chemical rockets to provide a reorientation maneuver to "collect" the liquid propellant at the end of the tank away from the vent. The low-level acceleration criteria for controlling the liquids are based on studies conducted in the zero-gravity drop tower (ref. 3).

The problems of long-term space missions such as interplanetary flights, deep space probes, and orbital storage systems more acutely point up the need for basic understanding in the area of zero- and low-gravity venting. The short-term cryogenic storage requirements of the Saturn and Centaur vehicles yield optimum weight system designs when the cryogenic boiloff is sacrificed in lieu of additional insulation. For long-term storage of cryogenics, insulation systems will be improved such that the vented propellant vapor will not be sufficient to supply propellant settling, and the use of auxiliary thrusters will place too large a weight penalty on the vehicle. Unless a device such as a liquid propellant thermal conditioning system (ref. 4) is employed, propellant control becomes mandatory. However, the application of a thermal conditioning system may add excessive weight penalties and complexity.

If some type of internal surface tension devices are included in the propellant tank to maintain liquid-vapor interface control, it would appear that venting during long-term space missions could be considered on a continuous basis. If the vent rate is very low, pressure control may be accomplished without disturbing the liquid bulk since liquid-vapor interface evaporation alone will supply the required vapor for venting. The objective of this study is to predict the pressure response of a saturated liquid-vapor system when undergoing a venting or depressurization process in zero gravity (weightlessness) at low vent rates.

A venting analysis was formulated based on lumping the continuity and energy equations governing the vapor space. The analysis is not limited to any particular tank shape or contained liquid.

The analysis includes interfacial mass transfer based on an infinitely planer (flat surface) conduction analysis (refs. 5 and 6). Interfacial mass transfer is often neglected for rapid venting, but for low vent rates the effect of interface mass transfer on the pressure response is significant. The pressure response for rapid venting is usually based on the adiabatic decompression venting model.

The pressure responses determined from the venting model which includes interface mass transfer are compared with the results from the adiabatic decompression venting model and the pressure responses obtained from short duration (5 sec nominally) drop tower tests conducted at the Lewis zero-gravity facility. Some qualitative information concerning bulk boiling similar to that obtained in reference 7 is also presented.

The work presented herein is concerned primarily with low vent rates in contrast to reference 8 in which larger vent rates (more than one ullage/sec) were of interest. Reference 8 presents experimental zero-gravity data for both refrigerant Freon 11 and liquid hydrogen. The test fluids used for this study include the refrigerants Freon 11

(R11), octofluorocyclobutane (RC318), and n-butane (R600). These fluids were chosen because they provide a range of heat-transfer properties and are saturated at room temperature and pressures only slightly above atmospheric.

SYMBOLS

A	area, m^2
C_D	discharge coefficient
C_V	specific heat at constant volume, J/(kg)(K)
F_1, F_2	functions
h	specific enthalpy, J/kg
h_{fg}	heat of vaporization, J/kg
K	thermal conductivity, W/(m)(K)
M	mass, kg
$\vec{n}$	unit normal vector
P	pressure, N/m^2
Q	volumetric flow rate, m^3/sec
q	heat flux, W/m^2
R	gas constant, (m)(N)/(kg)(K)
T	temperature, K
t	time, sec
U	internal energy, J
u	specific internal energy, J/kg
V	volume, m^3
v	velocity, m/sec
α	thermal diffusivity, m^2/sec
γ	ratio of specific heats
ρ	density, kg/m^3
$\xi(\bar{x})$	parameter

Subscripts:

1	initial state
2	state for times, $t > 0$
adia	adiabatic decompression computation
anal	analytical including interface mass transfer
exp	experimental
f	final
l	liquid
o	vented vapor
s	liquid-vapor surface
sat	saturation conditions
v	contained vapor

APPARATUS AND PROCEDURE

The Lewis zero-gravity facility was used to obtain the experimental data for this investigation. A complete description of the facility, the experiment package, and procedures for conducting the tests can be found in appendix A. The venting tests were conducted with right-circular cylindrical containers having flat ends as shown in figure 1. These test containers were fabricated from acrylic plastic.

The liquids employed in the tests were refrigerant 11 (CCl_3F), refrigerant C318 (C_4F_8), and refrigerant 600 ($CH_3CH_2CH_2CH_3$). Refrigerant 600 is commonly known as n-butane and refrigerant 11 is commonly known as Freon 11 or Genetron 11. The pertinent thermodynamic properties for all these fluids, such as enthalpy, specific volume, and entropy, can be found in standard refrigeration tables (ref. 9). All three of these fluids were found to exhibit a nearly 0° static contact angle on the test container surface, and are, therefore, representative of typical liquid propellants. The area of the liquid surface (5.57×10^{-3} m^2) is simply the area of a hemisphere having a radius equal to that of the tank since the venting sequence occurs during weightlessness. The tank pressure and the temperature in the vicinity of the liquid-vapor interface were monitored continuously before the drop test to ensure reaching nearly saturated conditions. The tank pressure was recorded during the drop test along with high-speed motion pictures. After releasing an experiment package, a maximum of 1.9 seconds was allowed for the liquid to achieve the hemispherical zero-gravity interface configuration; the timers then activated the vent sequence for approximately 3 seconds.

ANALYSIS

Adiabatic Decompression Venting Model

The pressure reduction of a tank containing only a perfect gas during the adiabatic withdrawal of that gas is calculated in order to make comparisons with a venting model which includes interfacial mass transfer. Conservation of mass is applied in the following manner: The rate of decrease of mass in the tank is set equal to the withdrawal rate where the volumetric withdrawal rate Q is assumed constant. When proceeding along the lines of the analysis presented in appendix B, substituting equation (B16), which is

$$\frac{P_1 T_2}{P_2 T_1} = e^{Qt/V_v}$$

into equation (B11), which is

$$\frac{T_2}{T_1} = e^{-QRt/V_v C_V}$$

leads to the following expression for the pressure reduction during an adiabatic decompression:

$$\frac{P_2}{P_1} = e^{-\gamma Qt/V_v} \tag{1}$$

Interface Mass Transfer Venting Model

At time zero, the venting process is assumed to start with initially saturated vapor exiting through the vent to a vacuum. A schematic of the venting system at various instances of time is shown in figure 2. The initial thermodynamic state of the vapor and liquid are known (saturated conditions). The pressure decrease within the container during venting causes mass to be transferred across the liquid-vapor interface. As venting continues, it is assumed that only vapor passes through the vent line. The analysis is based on a flat interface shape. However, in order to compare the model with the experimental data the area of the hemispherical surface is used for the analysis.

The overall system is divided into two separate control volumes - the vapor and the liquid regions. The vapor region consists of the region above the liquid surface, and its volume is a function of the liquid height. The vented vapor M_o is taken from this region. The mass transfer terms associated with the vapor region are shown in figure 3. As the liquid evaporates during a pressure reduction, some mass M_s is transferred to the vapor region causing the volume of the liquid region (see fig. 4) to vary slightly with time. It is assumed that no boiling occurs within the bulk liquid.

Derivation of Venting Equations

In applying the continuity and energy conservation equations, the volume V, which appears in the equations, is fixed since actual volume variations due to mass transfer will be small. The continuity equation is

$$\int_V \frac{\partial \rho}{\partial t} dV + \int_A \rho \vec{v} \cdot \vec{n} \, dA = 0 \tag{2}$$

$$\frac{d}{dt}\int_V \rho \, dV = -\int_A \rho \vec{v} \cdot \vec{n} \, dA \tag{3}$$

For the vapor region, equation (3) becomes

$$\frac{dM_v}{dt} = \dot{M}_s - \dot{M}_o \tag{4}$$

For the liquid region,

$$\frac{dM_l}{dt} = -\dot{M}_s \tag{5}$$

If the internal energy is assumed to be only a function of time, the energy equation in integral form is

$$\frac{d}{dt}\int_V \rho u \, dV + \int_A \rho u \vec{v} \cdot \vec{n} \, dA = -\int_A P\vec{v} \cdot \vec{n} \, dA - \int_A \vec{q} \cdot \vec{n} \, dA \tag{6}$$

Using the relation

$$h = u + \frac{P}{\rho} \tag{7}$$

in equation (6) yields the following form of the energy equation with $\vec{q} = 0$ (valid only for short test times):

$$\frac{d}{dt}\int_V \rho h \, dV - \frac{d}{dt}\int_V P \, dV = -\int_A \rho h \vec{v} \cdot \vec{n} \, dA - \int_A \vec{q} \cdot \vec{n} \, dA \tag{8}$$

For the vapor region, equation (8) becomes

$$\frac{d}{dt}(M_v h_v) - V_v \frac{dP_2}{dt} = \dot{M}_s h_{v,s} - \dot{M}_o h_v \tag{9}$$

For the liquid region,

$$\frac{d}{dt}(M_l h_l) - V_l \frac{dP_2}{dt} = -\dot{M}_s h_{l,s} \tag{10}$$

For the bulk liquid region, it is assumed that the initial and final temperatures during venting are identical and equal to T_1. The temperature at the liquid-vapor interface is $T_{2,sat}$, which is the saturation temperature corresponding to the ullage pressure P_2. The addition of equations (9) and (10), which is not independent of the mass transferred across the liquid-vapor interface, yields the product of the interface mass transfer rate and the latent heat of vaporization $\dot{M}_s h_{fg}$. The temperature of the vapor is also assumed to be $T_{2,sat}$, which is the saturation temperature corresponding to the ullage pressure. Since the mass transferred across the liquid-vapor interface enters at the saturation temperature, an adiabatic decompression computation was performed to show that the vapor initially in the control volume remains nearly saturated during a pressure reduction. This analysis was performed for the three fluids employed, and a sample calculation is contained in appendix C. The enthalpy of the vapor h_v is to be evaluated at the saturated conditions. Since the vapor region is of primary interest, the governing equations of the vapor region are rewritten as follows:

Continuity vapor:

$$\frac{dM_v}{dt} = \dot{M}_s - \dot{M}_o \tag{11}$$

Energy conservation vapor:

$$\frac{d}{dt}(M_v h_v) - V_v \frac{dP_2}{dt} = h_v(\dot{M}_s - \dot{M}_o) \tag{12}$$

Expressions for the mass transfer terms which appear in equations (11) and (12) are now examined in detail.

The mass flow rate through the vent $\dot{M}_o$ is determined by using the classical choked flow analysis. Since the vented gas goes directly into a vacuum, the choked flow assumption is valid and the mass flow rate is a function of upstream thermodynamic properties and an experimentally determined discharge coefficient (see table I). As discussed previously, the ullage pressure is a time-dependent quantity. Therefore, it follows that the vent mass flow rate will vary with time.

Analytical expression for $\dot{M}_s$. - A conduction analysis by Thomas and Morse (ref. 6) was applied to the interfacial mass transfer process occurring during depressurization for an infinitely planer (liquid-vapor) interface. The following expression was obtained from this analysis for the mass transfer rate:

$$\dot{M}_s = A_s \rho_l \left(\frac{\alpha_l}{t}\right)^{1/2} \left|\xi_l(\bar{x})\right| \tag{13}$$

where $\xi_l(\bar{x})$ satisfies the transcendental equation

$$\sqrt{\pi\alpha_l}\,\rho_l h_{fg} \xi_l(\bar{x}) = \frac{K_v(T_{2,sat} - T_{2,v})}{\sqrt{\alpha_v}} \frac{\exp\left\{\left(-\frac{\alpha_l}{\alpha_v}\right)\left[\left(\frac{\rho_l}{\rho_v}\right)\xi_l(\bar{x})\right]^2\right\}}{\operatorname{erfc}\left[\left(\frac{\rho_l}{\rho_v}\right)\sqrt{\frac{\alpha_l}{\alpha_v}}\,\xi_l(\bar{x})\right]} + \frac{K_l(T_{2,sat} - T_1)\exp\left[-\xi_l^2(\bar{x})\right]}{\sqrt{\alpha_l}\left[1 + \operatorname{erf}\xi_l(\bar{x})\right]} \tag{14}$$

TABLE I. - SUMMARY OF PARAMETERS

Refrigerant	Test	Initial filling, percent liquid	Initial vapor volume, m^3	Nozzle diameter, m	Discharge coefficient, C_D	Reduced flow rate, Q/V_{v_1}, ullage/sec	Initial ullage pressure, P_1, N/m^2	Initial ullage temperature, T_1, K	Final experimental ullage pressure, N/m^2	Final analytical ullage pressure, N/m^2	Final adiabatic ullage pressure, N/m^2	Dimensionless experimental pressure drop, $\Delta P_{exp}/P_1$	Dimensionless analytical pressure drop, $\Delta P_{anal}/P_1$	Dimensionless adiabatic pressure drop, $\Delta P_{adia}/P_1$
11	1	32	1.93×10^{-4}	0.406×10^{-3}	0.64	0.035	8.96×10^4	294.3	8.62×10^4	8.16×10^4	7.97×10^4	0.04	0.09	0.11
	2	29	2.01	.889	.69	.17	8.79	294.7	7.03	5.63	4.94	.20	.36	.44
	3	33	1.90	1.07	.86	.33	9.10	293.7	6.07	4.07	3.01	.33	.55	.67
	4	32	1.93	1.32	.875	.51	9.72	296.5	5.38	2.94	1.63	.45	.70	.83
	5	32	1.93	1.93	.77	1.12	10.1	295.4	4.14	1.31	.15	.59	.88	.99
C318	6	33	1.90×10^{-4}	0.406×10^{-3}	0.64	0.030	27.9×10^4	295.9	26.9×10^4	25.5×10^4	25.25×10^4	0.04	0.09	0.10
	7	34	1.87	.889	.69	.16	30.3	298.7	22.1	19.1	17.8	.27	.37	.41
	8	36	1.81	.889	.69	.165	29.0	297.3	21.0	18.0	16.7	.28	.38	.42
	9	34	1.87	1.07	.86	.29	30.0	297.3	17.2	13.1	11.4	.43	.56	.62
	10	35	1.84	1.32	.875	.455	29.0	296.3	13.0	8.10	6.35	.55	.72	.78
600	11	32	1.93×10^{-4}	0.330×10^{-3}	0.77	0.041	23.3×10^4	297.0	21.7×10^4	20.8×10^4	20.3×10^4	0.07	0.11	0.13
	12	35	1.84	.711	.81	.21	22.8	294.7	16.5	12.8	11.3	.28	.44	.50
	13	34	1.87	.889	.69	.27	21.0	293.7	14.8	10.0	8.50	.30	.52	.60
	14	35	1.84	.889	.69	.28	24.0	296.7	16.4	11.2	9.45	.32	.53	.61
	15	34	1.87	1.07	.86	.49	22.8	296.8	10.7	6.30	4.50	.53	.72	.80
	16	34	1.87	1.93	.77	1.31	23.6	297.0	5.65	1.52	.63	.76	.94	.97

where T_1 is the liquid temperature, $T_{2,sat}$ the liquid-vapor interface temperature, and $T_{2,v}$ the vapor temperature. Thomas and Morse show that if the expression for $\xi_l(\bar{x})$ is solved explicitly for $\xi_l(\bar{x})$ by expanding both the error functions and exponentials for small $\xi_l(\bar{x})$ one obtains

$$\xi_l(\bar{x}) = \frac{\dfrac{K_l(T_{2,sat} - T_1)}{\sqrt{\alpha_l}} + \dfrac{K_v(T_{2,sat} - T_{2,v})}{\sqrt{\alpha_v}}}{\sqrt{\pi\alpha_l}\,\rho_l h_{fg} - \dfrac{2K_v(T_{2,sat} - T_{2,v})}{\sqrt{\pi\alpha_v}}\dfrac{\rho_l}{\rho_v}\sqrt{\dfrac{\alpha_l}{\alpha_v}} + \dfrac{2K_l(T_{2,sat} - T_1)}{\sqrt{\pi\alpha_l}}} \tag{15}$$

Now let $T_{2,sat} = T_{2,v}$ (as per our stated assumption and appendix C verification):

$$\xi_l(\bar{x}) = \frac{\sqrt{\pi}\,K_l(T_{2,sat} - T_1)}{\pi\alpha_l\rho_l h_{fg} + 2K_l(T_{2,sat} - T_1)} \tag{16}$$

Let

$$F_1 = \pi\alpha_l\rho_l h_{fg} \tag{17}$$

and

$$F_2 = 2K_l(T_{2,sat} - T_1) \tag{18}$$

TABLE II. - TYPICAL PROPERTIES FOR TEST FLUIDS AT 297 K

Refrigerant	Thermal conductivity of liquid, K_l, W/(m)(K)	Liquid density, ρ_l, kg/m^3	Thermal diffusivity of liquid, α_l, m^2/sec	Heat of vaporization, h_{fg}, J/kg
R11	0.0866	1480	6.74×10^{-8}	1.84×10^{5}
RC 318	.0433	1500	2.56	1.07
R600	.1056	575	7.88	3.70

Typical values of F_1 and F_2 and hence the ratio F_2/F_1 are now computed. This computation was based on the largest temperature change of the tests that were performed for each fluid. The resulting values of F_2/F_1 were 0.071 for R11, 0.150 for RC318, and 0.157 for R600 (table II). Hence, the largest error in neglecting F_2 with respect to F_1 is 16 percent. Therefore,

$$\xi_l(\bar{x}) \cong \frac{K_l(T_{2,sat} - T_1)}{\sqrt{\pi}\,\alpha_l \rho_l h_{fg}} \tag{19}$$

Equation (19) can be substituted into equation (13) to obtain the following approximate solution for the interface mass transfer rate:

$$\dot{M}_s \cong \frac{A_s K_l (T_1 - T_{2,sat})}{\sqrt{\pi}\,h_{fg}} \sqrt{\frac{1}{\alpha_l t}} \tag{20}$$

By definition

$$K_l = \alpha_l C_{p,l} \rho_l \tag{21}$$

Therefore,

$$\dot{M}_s \cong \frac{A_s \rho_l C_{p,l} (T_1 - T_{2,sat})}{\sqrt{\pi}\,h_{fg}} \sqrt{\frac{\alpha_l}{t}} \tag{22}$$

When combined with the appropriate initial and boundary conditions, equations (11), (12), and (22) provide a complete thermodynamic description of the vapor space. These equations, along with equation (1) which gives the pressure reduction during an adiabatic decompression, were solved using a computer program (appendix D) which employed a calculation procedure using 60 time intervals. A comparison of the solutions to these equations with experimental data is presented in the RESULTS AND DISCUSSION section.

RESULTS AND DISCUSSION

Pressure Decay Characteristics

During space missions involving the use of cryogenic liquids, the maximum allowable tank pressure and the thermal environment dictate such items as venting times and insulation requirements. Consequently, the pressure response of the tank ullage during a venting sequence in space is an important parameter to be considered. A typical ullage pressure response for RC318 during one of the experimental tests is shown in figure 5. As previously mentioned in the APPARATUS AND PROCEDURE section, the experiment tank contents were allowed sufficient time to reach a saturated equilibrium condition corresponding to the ambient temperature in the test facility. The initial pressure for the test shown in figure 5 is 29×10^4 newtons per square meter. A time duration of 1.9 seconds was then allowed during free-fall so that the liquid-vapor interface could attain a hemispherical equilibrium configuration. Note that the tank pressure remains constant during this time period as expected. At 1.9 seconds after the initiation of the test, the vent was opened and vapor passed through the vent line for a period of 3 seconds. The final ullage pressure reached 13×10^4 newtons per square meter as seen in figure 5.

In table I, the test parameters for the 16 no-boiling zero-gravity tests conducted during this program are shown. Note that test 10 is the typical test whose pressure characteristics are shown in figure 5.

Comparison of Experiment With Theory

As a direct result of one of the assumptions made in the analyses, namely, that the vapor remains saturated during a depressurization or venting sequence, the mass conservation equation (eq. (11)) and the energy conservation equation (eq. (12)) remain uncoupled. Hence, the solution to either equation along with the corresponding expressions for the vent mass flow rate and interface mass transfer, using the proper boundary and initial conditions, results in identical solutions. Computer programs were run with each separately and yielded similar results. The test conditions and the results from the computer program are contained in table I. The final ullage pressure, based on the interface mass transfer venting model, is under the column labeled "Final analytical ullage pressure." The tabulated results for the final ullage pressure based on the adiabatic decompression venting model are under the column labeled "Final adiabatic ullage pressure." In all cases the adiabatic calculation yielded a lower final ullage pressure than for the venting model calculation which included interfacial mass transfer. The difference is due to the fact that the addition of mass from the interface into the vapor space would not allow the tank pressure to decrease as rapidly. In all tests, for both the adiabatic decompression and the venting model calculation including mass transfer, the computed final ullage pressures were lower than the corresponding experimental values.

A graphical comparison of the three previously mentioned pressure drops nondimensionalized in terms of the initial pressure ($\Delta P/P_1$) is presented as a function of the reduced flow rate (Q/V_{v_1}) in figures 6 to 8. The reduced flow rate is the average volumetric flow rate divided by the initial vapor volume. (These two parameters are also tabulated in table I). Figure 6 presents the results for refrigerant 11, figure 7 presents the results for refrigerant C318, and figure 8 presents the results for refrigerant 600. The experimental and analytical data points contained on these three curves are for the 0.06 meter diameter cylindrical tank having a nominal 33 percent by volume initial filling of liquid.

Figures 6 to 8 indicate that the analysis which includes interfacial mass transfer shows approximately 25 to 35 percent improvement with respect to the final ullage pressure prediction in comparison with the adiabatic computation. However, there still exists a significant gap between experiment and theory.

The inclusion of the term F_2 in equation (16) would lead to larger interfacial mass transfer rates since the final temperature ($T_{2,sat}$) is always less than the initial temperature (T_1). Since the discrepancy between experiment and analysis is the result of an insufficient amount of interfacial mass transfer, inclusion of the term F_2 would result in an improvement. However, this was earlier judged to be a minor effect. Of major importance is the fact that an infinitely planer conduction analysis attributable to Thomas and Morse (ref. 6) was employed. This, in effect, neglects heat conduction from the side walls. Since the liquid-vapor interface was hemispherical in shape there exists a very large temperature gradient and, hence, significant heat-transfer rate through the thin liquid surface on the walls in the neighborhood of the leading edge. It would appear that an improvement in the analysis that included both curved interfaces and finite walls would yield higher mass transfer rates and, thus, lead to a much better agreement between analysis and experiment.

Another factor which could contribute to increasing the interfacial mass transfer is the liquid motion caused by the initial change from a normal-gravity to a zero-gravity configuration and as a response to the venting disturbance. However, it would probably be impossible to incorporate this effect into a venting model analysis.

Bulk Boiling

Any complete study of venting under any gravitational conditions should include the possibility of boiling occurring within the liquid bulk. The analysis which appears in this report does not apply to situations in which bulk boiling occurs. Hence, all the data points which appear in table I are for cases wherein no bulk boiling was observed. The problem of predicting the inception of bulk boiling is presently without solution. Certainly the inception point would depend on the tank surface conditions which determine the size and distribution of nucleation sites and also the properties of the particular fluid. While the intent of this report was not geared directly toward a discussion of the prediction of the aforementioned phenomenon, it did arise in one test case.

The photographic sequence for test 10 (refrigerant C318) is shown in figure 9. Note that the average vent rate for this particular test was $Q/V_{v_1} = 0.5$ ullage volume per second. In this test no bulk boiling occurred. However, as seen in figure 10, for an average vent rate of 1.0 ullage volume per second, for RC318, extensive bulk boiling occurs. The liquid-vapor interface is pushed toward the vent as a result of the growth of two rather large vapor bubbles. These vapor bubbles do not break the liquid-vapor interface and cause large surface disturbances as the vent sequence continues. The venting model analysis cannot be applied to test cases where bulk boiling occurs since the liquid-vapor interface area is not only varying with time but would also be impossible to predict.

CONCLUDING REMARKS

An experimental investigation of venting cylindrical containers partially filled with initially saturated liquids under zero-gravity conditions was conducted in the NASA Lewis Research Center 5-second zero-gravity facility. The test fluids, refrigerants 11, C318, and 600, all possessed a near-zero contact angle on the container surface resulting in a hemispherical liquid-vapor interface shape in zero gravity. The experimental pressure responses were compared with pressure responses predicted by an adiabatic decompression venting model and a lumped system venting model which includes interfacial mass transfer.

For the tests which exhibited no bulk boiling the adiabatic decompression venting model predicted too large a pressure reduction by nearly a factor of two. The addition of the effects of interfacial mass transfer to a lumped system venting model, based on a conduction analysis for an infinitely planer (flat) surface, resulted in approximately a 30-percent improvement in the determination of the ullage pressure response when compared to the adiabatic decompression venting model.

It is the authors' belief that the container walls act as a heat source and cause additional liquid evaporation thus reducing the experimental pressure decay. In order to improve the agreement between experimental and analytical venting system results, the infinitely planer surface analytical approach presented in this report would have to be modified to account not only for the container walls but also the curvature of the liquid-vapor interface.

Lewis Research Center,
National Aeronautics and Space Administration,
Cleveland, Ohio, August 14, 1973,
909-72.

APPENDIX A

APPARATUS AND PROCEDURE

Test Facility

The experiment data for this study were obtained in the 5- to 10-second zero-gravity facility at the Lewis Research Center. A schematic diagram of this facility is shown in figure 11. The facility consists of a concrete-lined 8.5-meter-diameter shaft that extends 155 meters below ground level. A steel vacuum chamber, 6.1 meters in diameter and 143 meters high, it contained within the concrete shaft. The pressure in this vacuum chamber is reduced to 13.3 newtons per square meter by utilizing the Center's wind tunnel exhaust system and an exhauster system located in the facility.

The ground-level service building has, as its major elements, a shop area, a control room, and a clean room. Assembling, servicing, and balancing the experiment vehicle are accomplished in the shop area. Tests are conducted from the control room (see fig. 12) which contains the exhauster control system, the experiment vehicle predrop checkout and control system, and the data retrieval system. Those components of the experiment which are in contact with the test fluid are prepared in the facility's class 10,000 clean room. The major elements of the clean room are an ultrasonic cleaning system (fig. 13(a)) and a class 100 laminar-flow station (fig. 13(b)) for preparing those experiments requiring more than normal cleanliness.

Mode of operation. - The zero-gravity facility has two modes of operation. One is to allow the experiment vehicle to free-fall from the top of the vacuum chamber, which results in nominally 5 seconds of free-fall time. The second mode is to project the experiment vehicle upwards from the bottom of the vacuum chamber by a high pressure pneumatic accelerator located on the vertical axis of the chamber. The total up-and-down trajectory of the experiment vehicle results in nominally 10 seconds of free-fall time. The 5-second mode of operation was used for this experimental study.

In either mode of operation, the experiment vehicle falls freely; that is, no guide wires, electrical lines, and so forth are connected to the vehicle. Therefore, the only force (aside from gravity) acting on the freely falling experiment vehicle is due to residual air drag. This results in an equivalent gravitational acceleration acting on the experiment which is estimated to be of the order of 10^{-5} g maximum.

Recovery system. - After the experiment vehicle has traversed the total length of the vacuum chamber, it is decelerated in a 3.6-meter-diameter, 6.1-meter-deep container which is located on the vertical axis of the chamber and filled with small pellets of expanded polystyrene. The deceleration rate (averaging 32 g's) is controlled by the flow of pellets through the area between the experiment vehicle and the wall of the deceleration container. This deceleration container is mounted on a cart which can be retracted prior to utilizing the 10-second mode of operation. In this mode of operation, the cart is deployed after the experiment vehicle is projected upward by the pneumatic accelerator. The deceleration container mounted on the cart is shown in figure 14.

Experiment Vehicle

The experiment vehicle consisted of two basic sections (see fig. 15). The experiment section is contained in the cylindrical midsection and the telemetry section is contained in the top fairing.

Experiment. - The experiment section consisted of the test container tray (see fig. 16) plus electrical power and control system equipment mounted in the cylindrical section of the experiment vehicle. The test container tray includes the test container, camera, and lighting and timing systems. The vent system which included a solenoid valve and various sized nozzles and orifices was mounted above the test container. The solenoid valve opened during the test drop and vapor was vented either to the low pressure test chamber or to a collection tank also at a low pressure. The ensuing venting procedure was recorded by a high-speed motion picture camera. Elapsed time was obtained from a digital clock.

Telemetry system. - The on-board telemetry system is an FM/FM system with 18 continuous channels. During a test drop, telemetry is used to continuously record the output from two low-gravity accelerometers and the tank pressure. The initial temperature in the vicinity of the liquid-vapor interface is also obtained from the recording system, but the temperature data obtained during the test was not used due to the questionable response time of the transducer. The accuracy of all temperatures quoted in this report is conservatively estimated to be $\pm 1.5^{\circ}$, while the accuracy of all pressures is estimated to be ± 1 newton per square centimeter.

Test Procedure

Cleaning, filling, and hermetic sealing the test containers were conducted in the zero gravity facility's clean room (fig. 13). Contamination of the liquid and cylinder, which could alter the surface tension and contact angle, was carefully avoided. The test cylinders were cleaned ultrasonically in a detergent-water solution, rinsed with a distilled-water-methanol solution, and dried in a warm air dryer. The test cylinders were rinsed with the test liquid, filled to the desired liquid depth, and sealed to prevent contamination. They were then mounted on the test container tray. During the test, a predetermined time increment was allowed (1.9 sec maximum) so that the liquid-vapor interface could approach its low-gravity equilibrium shape. After the formation time, the solenoid valve was opened and the vapor vented to vacuum for 3 seconds.

Electrical timers on the experiment vehicle are set to control the initiation and duration of all functions programmed during the drop. The experiment vehicle is balanced about its vertical axis to ensure an accurate drop trajectory.

The vehicle is then positioned at the top of the vacuum chamber as shown in figure 17. It is suspended by the support shaft on a hinged-plate release mechanism. During vacuum chamber pumpdown and prior to release, monitoring of experiment vehicle systems is accomplished through an umbilical cable attached to the top of the support shaft. Electrical power is aupplied from ground equipment. The system is then switched to internal power a few minutes before release. The umbilical cable is remotely pulled from the support shaft 0.5 second prior to release. The vehicle is released by pneumatically shearing a bolt that holds the hinged plate in the closed position. No measurable disturbances are imparted to the experiment vehicle by this release procedure.

The total free-fall test time obtained in this mode of operation is 5.16 seconds. During the test drop, the vehicle's trajectory and deceleration are monitored in closed-circuit television. Following the test drop, the vacuum chamber is vented to the atmosphere and the experiment vehicle is returned to ground level.

APPENDIX B

ADIABATIC DECOMPRESSION VENTING MODEL

A container of gas at some high pressure is assumed. At time zero, a valve is opened allowing the gas to escape. The temperature and pressure dependence with time will be examined. An adiabatic process is assumed ($q = 0$) so that the rate of change of internal energy is equal to the rate of energy removal:

$$\frac{dU}{dt} = \frac{dM}{dt}(h) \tag{B1}$$

where

$$U = Mu = MC_V T \tag{B2}$$

and

$$h = u + RT \tag{B3}$$

Expanding equation (B2) gives

$$\frac{dU}{dt} = \left(\frac{\partial U}{\partial t}\right)\left(\frac{dT}{dt}\right) + \left(\frac{\partial U}{\partial M}\right)\left(\frac{dM}{dt}\right) \tag{B4}$$

and

$$\frac{dU}{dt} = MC_V\left(\frac{dT}{dt}\right) + u\left(\frac{dM}{dt}\right) \tag{B5}$$

When equation (B1) is used, equation (B5) becomes

$$h\,\frac{dM}{dt} = MC_V\left(\frac{dT}{dt}\right) + u\left(\frac{dM}{dt}\right) \tag{B6}$$

The rate of change of mass leaving the container can be expressed in terms of the volumetric flow rate Q as follows:

$$-\frac{dM}{dt} = \frac{PQ}{RT} \tag{B7}$$

when Q is assumed to be a constant in time. Substituting equation (B7) into equation (B6) gives

$$-\frac{PQ}{RT}(u + RT) = MC_V\left(\frac{dT}{dt}\right) - \frac{PQ}{RT} u \tag{B8}$$

which becomes after some simplification

$$\frac{dT}{T} = -\frac{Q}{V_v}\frac{R}{C_V} dt \tag{B9}$$

Integrating gives

$$\int_{T_1}^{T_2} \frac{dT}{T} = -\frac{Q}{V_v}\frac{R}{C_V}\int_{t_1}^{t_2} dt \tag{B10}$$

The solution of the previous equation is

$$T_2 = T_1 e^{-QRt/V_v C_V} \tag{B11}$$

Now the time dependence of the ullage pressure is derived by employing conservation of mass. The rate of decrease of mass in the container equals the withdrawal rate which the volumetric removal rate is assumed constant. The rate of change of mass leaving the container is expressed in terms of Q by equation (B6) and M, of course, is related to the other thermodynamic variables through the perfect gas law

$$M = \frac{PV_v}{RT} \tag{B12}$$

Therefore, expanding equation (B12) gives

$$\frac{dM}{dt} = \left(\frac{\partial M}{\partial P}\right)\left(\frac{dP}{dt}\right) + \left(\frac{\partial M}{\partial T}\right)\left(\frac{dT}{dt}\right) \tag{B13}$$

Using previous relations in equation (B12) gives

$$-\frac{PQ}{RT} = \frac{V_v}{RT}\left(\frac{dP}{dt}\right) - \frac{PV_v}{RT^2}\left(\frac{dT}{dt}\right) \tag{B14}$$

Rewriting equation (B14) gives

$$\frac{Q}{V_v}\,dt = -\frac{dP}{P} + \frac{dT}{T} \tag{B15}$$

Integration yields

$$\frac{P_1T_2}{P_2T_1} = e^{Qt/V_v} \tag{B16}$$

APPENDIX C

EXAMINATION OF ASSUMPTION OF SATURATED VAPOR

The procedure used to check the validity of the assumption of the vapor temperature remaining saturated was to calculate T_2/T_1 from equation (B11). To accomplish this, typical values of Q, V_v, and t were chosen (table III). The value of T_2/T_1 thus

TABLE III. - TYPICAL FLUID PROPERTIES AND

EXPERIMENTAL VALUES FROM TEST 2

Fluid properties	
Liquid	refrigerant 11
Specific heat at constant volume, C_V, J/(kg)(K)	528
Gas constant, R, J/(kg)(K)	58.6
Time, t, sec	3
Volume of vapor, V_v, m^3	2.01×10^{-4}
Average volumetric flow rate, Q, m^3/sec	0.342×10^{-4}
Temperature, T, K	294.7
Initial pressure, P_1, N/m^2	8.79×10^4

found was substituted into equation (B16), and equation (B16) was solved for P_2/P_1. Finally, the saturation pressure corresponding to T_2 is compared with the value of P_2 computed by means of equation (B16). Using these typical values in equation (B11) yields $T_2/T_1 = 0.945$. Therefore, T_2 equals 278.5 K, which corresponds to a saturation pressure of 5.07×10^4 newtons per square meter. The ratio P_2/P_1 calculated from equation (B16) is found to be 0.563. Hence, $P_2 = 4.94\times10^4$ newtons per square meter. Therefore, the assumption of saturated vapor throughout the venting sequence appears reasonable.

APPENDIX D

COMPUTER PROGRAM

The computer program used for numerically solving equations (11), (12), and (22) consists of a main program and four subroutines. The subroutines DD, CURVE, DERIV, and RKGS make available the Runge-Kutta method for the numerical solution of an ordinary first-order differential equation with nonconstant coefficients, the independent variable in all cases being time. A calculation procedure was employed which divided the 3-second test time into 60 intervals in order to improve the accuracy of the computations. Also included in the computer program was the solution of equation (1) which yields the pressure decrease based on the adiabatic decompression venting model. This appendix includes a dictionary of the FORTRAN symbols used, the program listing, and a complete input/output list for one test. A typical flow chart is shown in figure 18. All of the data were analyzed using the computer program with only slight variations due to the different sources and formats of the thermodynamic properties for the three fluids.

Dictionary of FORTRAN Symbols

FORTRAN symbol	Engineering symbol	
AT	A	area of vent nozzle at throat
AS	A_s	liquid-vapor surface area
CD	C_D	discharge coefficient
CPL	$C_{p,l}$	specific heat of liquid
GO	G_o	acceleration due to gravity
H	h	specific enthalpy
HFG	h_{fg}	heat of vaporization
K	K	thermal conductivity
MV	$\dot{M}_v$	mass flow rate of vented vapor
MMT	$\dot{M}_s$	mass flow rate across liquid-vapor surface
P2, Y(1)	P_2	ullage pressure based on venting model
Q	Q	volumetric flow rate

FORTRAN symbol	Engineering symbol	
T,X	t	time
T1	$T_{v,1}$	initial ullage temperature
T2	$T_{sat,2}$	saturation temperature corresponding to P_2
VV	V	volume
Y3	P_2	ullage pressure based on adiabatic decompression
ALPHAL	α_l	liquid thermal diffusivity
RHOL	ρ_l	liquid density
RHOV,Y(2)	ρ_v	vapor density

PROGRAM LISTING

```
      EXTERNAL DD
      COMMON P2I,MV,Q,Y3,AT,AS,CPL,ALPHAL,VV,RHOL,T1,CD,GO,KODE
      DIMENSION Y(2),DY(2),TITLE(12)
      REAL MV
    2 READ(5,102) (TITLE(I),I=1,12)
      READ (5,105) P2,RHOV,AT,AS,CPL,ALPHAL,VV,RHOL,T1,CD,GO
C     KODE=1    MMT CALCULATED        KODE=0        MMT=0.0
      KODE=0
      DO 3 II=1,2
C     INITIALIZE T  -  X
      X=0.00001
C     INITIALIZE P2  -  Y(1)
      Y(1)=P2
C     INITIALIZE RHOV  -  Y(2)
      Y(2)=RHOV
      P2I=Y(1)
      WRITE(6,100)
      WRITE(6,103) (TITLE(I),I=1,12)
      WRITE(6,104)
      WRITE(6,107) P2,RHOV,AT,AS,CPL,ALPHAL,VV,RHOL,T1,CD,GO,KODE
      WRITE (6,104)
      WRITE(6,106)
      DO 1 I=1,60
      XF=X+0.05
      CALL RKGS (X,XF,H,.1E-3,Y,DY,2,DD)
      WRITE(6,101) X,Y(1),MV,Q,Y3
    1 CONTINUE
      KODE=KODE+1
    3 CONTINUE
      GO TO 2
  100 FORMAT(120H1ZERO GRAVITY VENTING MASS BALANCE AND ENERGY BALANCE
     1                                         LABUS - AMLING          )
  101 FORMAT(10X,5G15.6)
  102 FORMAT(12A6)
  103 FORMAT(1HK,12A6)
```

```
104 FORMAT(1HK)
1C5 FORMAT(2F6.0,E6.2,7F6.0,F12.0)
106 FORMAT(1H0,14X,7HT (SEC),9X,2HP2,14X,2HMV,14X,1HQ,14X,2HY3)
107 FORMAT(5H0P2= ,G16.8/7H RHOV= ,G16.8/5H AT= ,G16.8/5H AS= ,G16.8/
   16H CPL= ,G16.8/9H ALPHAL= ,G16.8/5H VV= ,G16.8/7H RHOL= ,G16.8/5H
   2T1= ,G16.8/5H CD= ,G16.8/5H GO= ,G16.8/7H KODE= ,I2/)
    END

      SUBROUTINE DD (X,Y,DY)
C
C     HOMOGENEOUS DIFFERENTIAL EQUATION OF THE FIRST ORDER USING
C     RUNGE-KUTTA SOLUTION
C
      COMMON P2I,MV,Q,Y3,AT,AS,CPL,ALPHAL,VV,RHOL,T1,CD,GO,KODE
      DIMENSION COEFF1(5),COEFF2(5),COEFF3(5),COEFF4(5),COEFF5(5),
     1COEFF6(5),COEFF7(5),COEFF8(5),T(100),P2A(100),Y(2),DY(2)
C     R600 COEFFICIENTS
C     CURVE 1            RHOV VS. P
      DATA (COEFF1(I),I=1,5)/0.12715492E-01,0.10550608E-01,0.11994321E-0
     14,-0.61399911E-06,0.72537941E-08/
C     CURVE 2            T2 VS. P
      DATA (COEFF2(I),I=1,5)/-45.905340,7.8234674,-0.22653183,0.38259717
     1E-02,-0.25415846E-04/
C     CURVE 3            H2 VS. P
      DATA (COEFF3(I),I=1,5)/-633.91002,2.4116720,-0.65913194E-01,0.1050
     13420E-02,-0.65971124E-05/
C     CURVE 4            HFG VS. P
      DATA (COEFF4(I),I=1,5)/180.66624,-1.5806674,0.49739617E-01,-0.9392
     111366E-03,0.67298545E-05/
C     CURVE 5            K VS. P
      DATA (COEFF5(I),I=1,5)/-0.56075050E-03,4.9051085,-0.34892180E-01,
     10.71910064E-03,-0.59942675E-05/
      REAL MMT,MV,K
      SQRTPI=1.772438
C
C     COMPUTE MMT - USE THERMODYNAMIC CHARTS TO OBTAIN T2, AND HFG
C
      P2=Y(1)
      CALL CURVE(COEFF2,P2,T2)
      CALL CURVE(COEFF4,P2,HFG)
      MMT=0.0
      IF(KODE.EQ.0) GO TO 1
      MMT=    AS*RHOL*CPL*(T1-T2)*SQRT(ALPHAL/X    )/(SQRTPI*HFG*60.)
    1 CONTINUE
      CALL CURVE (COEFF5,P2,K)
      MV=CD*AT*K
C
C     COMPUTE DP2/DT USE THERMODYNAMIC CHARTS TO OBTAIN RHOV, RHOVP, AND
C     H2P
C
      CALL CURVE(COEFF1,P2,RHOV)
      CALL CURVE(COEFF3,P2,H2)
      CALL DERIV(COEFF1,P2,RHOVP)
      CALL DERIV(COEFF3,P2,H2P)
      DY(2)=((MMT-MV)/VV)
      DY(1)=DY(2)/RHOVP
      Q=MV/Y(2)
      Y3=P2I*EXP(-Q*X*1.11 /VV)
      RETURN
      END
```

```
      SUBROUTINE CURVE(COEFF,X,Y)
      DIMENSION COEFF(5)
      Y=COEFF(1)+X*(COEFF(2)+X*(COEFF(3)+X*(COEFF(4)+X*COEFF(5))))
      RETURN
      END
```

```
      SUBROUTINE DERIV(COEFF,X,DYDX)
      DIMENSION COEFF(5)
      DYDX=COEFF(2)+X*(2.0*COEFF(3)+X*(3.0*COEFF(4)+X*4.0*COEFF(5)))
      RETURN
      END
```

```
C
C        PARAMETERS
C
C        XO       INITAL VALUE FOR X, RETURNED AS XF NORMALLY
C        XF       FINAL VALUE FOR X
C        HH       NORMALLY RETURNED AS STEP SIZE USED NEAR XF
C                 RETURNED AS 0 IF MORE THAN 25 HALVINGS
C        ERR      UPPER ERROR BOUND , USED TO CONTROL STEP SIZE
C        Y        DEPENDENT VARIABLES, SET TO INITAL VALUES,
C                 RETURNED AT X=XF NORMALLY
C        DERY     DERIVATIVES DY/DX
C        NDIM1    NUMBER OF EQUATIONS IN SYSTEM
C        FCT      EXTERNAL SUBROUTINE WHICH CALCULATES DERIVATIVES
C                 CALL IS CALL FCT(X,Y,DERY)
      SUBROUTINE RKGS(XO,XF,HH,ERROR,Y,DERY,NDIM1,FCT)
      DIMENSION Y(1),DERY(1)
      DIMENSION AUX(7,20),A(4),B(4)
      DATA A /.5,.29289322,1.7071068,.16666667/
      DATA B /2.,1.,1.,2./
      NDIM = NDIM1
      ERR = ERROR
      X = XO
      XEND = XF
      H = (XEND-X)*.0625
C        CHECK ZERO
      IF(H.EQ.0.) GO TO 40
      CALL FCT(X,Y,DERY)
C
C
C     PREPARATIONS OF FIRST RUNGE-KUTTA STEP
      DO 3 I=1,NDIM
      AUX(1,I)=Y(I)
      AUX(2,I)=DERY(I)
      AUX(3,I)=0.
    3 AUX(6,I)=0.
      H=H+H
      IHLF=-1
```

```
      ISTEP=0
      IEND=0
C
C
C     START OF A RUNGE-KUTTA STEP
    4 IF((X+H-XEND)*H)7,6,5
C         GONE PAST, ADJUST H, SET IEND
    5 HH = H
      H = XEND - X
      IEND = 1
      GO TO 7
C         ON OR WITHIN TOLERANCE, SET IEND
    6 IEND  = 1
      HH = H
C
C         KEEP GOING
    7 ITEST = 0
    9 ISTEP=ISTEP+1
C
C
C     START OF INNERMOST RUNGE-KUTTA LOOP
      J=1
   10 AJ=A(J)
      BJ=B(J)
      CJ = AJ
      IF(J.EQ.4) CJ = .5
      DO 11 I=1,NDIM
      R1=H*DERY(I)
      R2=AJ*(R1-BJ*AUX(6,I))
      Y(I)=Y(I)+R2
      R2=R2+R2+R2
   11 AUX(6,I)=AUX(6,I)+R2-CJ*R1
      IF(J-4)12,15,15
   12 J=J+1
      IF(J-3)13,14,13
   13 X=X+.5*H
   14 CALL FCT(X,Y,DERY)
      GOTO 10
C     END OF INNERMOST RUNGE-KUTTA LOOP
C
C
C     TEST OF ACCURACY
   15 IF(ITEST)16,16,20
C
C     IN CASE ITEST=0 THERE IS NO POSSIBILITY FOR TESTING OF ACCURACY
   16 DO 17 I=1,NDIM
   17 AUX(4,I)=Y(I)
      ITEST=1
      ISTEP=ISTEP+ISTEP-2
   18 IHLF=IHLF+1
      X=X-H
      H=.5*H
      DO 19 I=1,NDIM
      Y(I)=AUX(1,I)
      DERY(I)=AUX(2,I)
   19 AUX(6,I)=AUX(3,I)
      GOTO 9
C
C     IN CASE ITEST=1 TESTING OF ACCURACY IS POSSIBLE
```

```
   20 IMOD=ISTEP/2
      IF(ISTEP-IMOD-IMOD)21,23,21
   21 CALL FCT(X,Y,DERY)
      DO 22 I=1,NDIM
      AUX(5,I)=Y(I)
   22 AUX(7,I)=DERY(I)
      GOTO 9
C
C     COMPUTATION OF TEST VALUE DELT
   23 DELT=0.
      DO 24 I=1,NDIM
   24 DELT = DELT + ABS(AUX(4,I)-Y(I))
      IF(DELT.LE.ERR) GO TO 28
C
C     ERROR IS TOO GREAT
      IF(IHLF.GT.25) GO TO 38
      DO 27 I=1,NDIM
   27 AUX(4,I)=AUX(5,I)
      ISTEP=ISTEP+ISTEP-4
      X=X-H
      IEND=0
      GOTO 18
C
C     RESULT VALUES ARE GOOD
   28 CALL FCT(X,Y,DERY)
      DO 29 I=1,NDIM
      AUX(1,I)=Y(I)
      AUX(2,I)=DERY(I)
      AUX(3,I)=AUX(6,I)
      Y(I)=AUX(5,I)
   29 DERY(I)=AUX(7,I)
   30 DO 31 I=1,NDIM
      Y(I)=AUX(1,I)
   31 DERY(I)=AUX(2,I)
      IF(IEND)32,32,39
C
C     INCREMENT GETS DOUBLED
   32 IHLF=IHLF-1
      ISTEP=ISTEP/2
      H=H+H
      IF(IHLF)4,33,33
   33 IMOD=ISTEP/2
      IF(ISTEP-IMOD-IMOD)4,34,4
   34 IF(DELT.GT..02*ERR) GO TO 4
      IHLF = IHLF - 1
      ISTEP=ISTEP/2
      H=H+H
      GOTO 4
C
C
   38 HH = 0.
      GO TO 40
   39 XO = X
   40 RETURN
      END
```

Typical Input/Output

```
ZERO GRAVITY VENTING MASS BALANCE AND ENERGY BALANCE

      VEHICLE MODEL - FLUID R600 (BUTANE)

P2=     34.8000002
RHOV=     0.37940000
AT=     0.66700000E-05
AS=     0.60000000E-01
CPL=     0.56000000
ALPHAL=     0.30800000E-02
VV=     0.65000000E-02
RHOL=     35.8099999
T1=     76.3000002
CD=     0.69000000
GD=     25051.6001
KODE=   0
```

T (SEC)	P2	MV	Q	Y3
0.500100E-01	34.29195	0.680602E-03	0.181917E-02	34.26353
0.100010	33.79093	0.671186E-03	0.181928E-02	33.73536
0.150010	33.29687	0.661893E-03	0.181938E-02	33.21528
0.200010	32.80970	0.652724E-03	0.181946E-02	32.70319
0.250010	32.32936	0.643677E-03	0.181954E-02	32.19896
0.300010	31.85576	0.634752E-03	0.181960E-02	31.70248
0.350010	31.38884	0.625947E-03	0.181965E-02	31.21364
0.400010	30.92852	0.617261E-03	0.181969E-02	30.73233
0.450010	30.47472	0.608694E-03	0.181973E-02	30.25843
0.500010	30.02737	0.600243E-03	0.181977E-02	29.79183
0.550010	29.58638	0.591908E-03	0.181979E-02	29.33243
0.600010	29.15167	0.583688E-03	0.181982E-02	28.88011
0.650010	28.72317	0.575580E-03	0.181984E-02	28.43476
0.700010	28.30080	0.567584E-03	0.181986E-02	27.99628
0.750010	27.88447	0.559698E-03	0.181987E-02	27.56456
0.800010	27.47410	0.551921E-03	0.181988E-02	27.13950
0.850010	27.06962	0.544251E-03	0.181989E-02	26.72100
0.900010	26.67094	0.536687E-03	0.181990E-02	26.30896
0.950010	26.27799	0.529228E-03	0.181991E-02	25.90328
1.000010	25.89069	0.521871E-03	0.181991E-02	25.50386
1.050010	25.50895	0.514616E-03	0.181991E-02	25.11061
1.100010	25.13270	0.507461E-03	0.181991E-02	24.72344
1.150010	24.76186	0.500405E-03	0.181990E-02	24.34226
1.200009	24.39635	0.493445E-03	0.181989E-02	23.96697
1.250009	24.03611	0.486582E-03	0.181988E-02	23.59750
1.300009	23.68105	0.479812E-03	0.181986E-02	23.23375
1.350009	23.33110	0.473136E-03	0.181984E-02	22.87564
1.400009	22.98619	0.466551E-03	0.181981E-02	22.52309
1.450009	22.64624	0.460057E-03	0.181977E-02	22.17602
1.500009	22.31118	0.453651E-03	0.181973E-02	21.83435
1.550009	21.98094	0.447332E-03	0.181968E-02	21.49800
1.600009	21.65546	0.441100E-03	0.181962E-02	21.16690
1.650009	21.33466	0.434953E-03	0.181955E-02	20.84098
1.700009	21.01848	0.428889E-03	0.181947E-02	20.52016
1.750009	20.70684	0.422907E-03	0.181938E-02	20.20437
1.800009	20.39969	0.417007E-03	0.181928E-02	19.89353
1.850009	20.09695	0.411186E-03	0.181917E-02	19.58759
1.900009	19.79857	0.405445E-03	0.181905E-02	19.28648
1.950009	19.50447	0.399780E-03	0.181891E-02	18.99012
2.000008	19.21461	0.394193E-03	0.181875E-02	18.69845
2.050008	18.92890	0.388680E-03	0.181858E-02	18.41141
2.100008	18.64731	0.383241E-03	0.181840E-02	18.12894
2.150008	18.36976	0.377876E-03	0.181819E-02	17.85097
2.200008	18.09620	0.372582E-03	0.181797E-02	17.57745
2.250008	17.82657	0.367359E-03	0.181773E-02	17.30831
2.300008	17.56082	0.362207E-03	0.181747E-02	17.04350
2.350008	17.29889	0.357123E-03	0.181719E-02	16.78295
2.400008	17.04072	0.352107E-03	0.181688E-02	16.52661
2.450008	16.78626	0.347158E-03	0.181656E-02	16.27443
2.500008	16.53546	0.342275E-03	0.181621E-02	16.02634
2.550008	16.28826	0.337457E-03	0.181583E-02	15.78230
2.600008	16.04462	0.332703E-03	0.181543E-02	15.54225
2.650007	15.80448	0.328013E-03	0.181501E-02	15.30614
2.700007	15.56780	0.323385E-03	0.181456E-02	15.07391
2.750007	15.33452	0.318818E-03	0.181408E-02	14.84551
2.800007	15.10460	0.314312E-03	0.181357E-02	14.62089
2.850007	14.87799	0.309866E-03	0.181303E-02	14.40001
2.900007	14.65464	0.305479E-03	0.181246E-02	14.18281
2.950007	14.43450	0.301150E-03	0.181186E-02	13.96924
3.000007	14.21754	0.296879E-03	0.181122E-02	13.75926

REFERENCES

1. Navickas, J.; and Madsen, R. A.: Propellant Behavior During Venting in an Orbiting Saturn S-IV-B Stage. Advances in Cryogenic Engineering. Vol. 13. K. D. Timmerhaus, ed. Plenum Press, 1968, pp. 188-198.

2. Lacovic, Raymond F.; Yeh, Frederick C.; Szabo, Steven V., Jr.; Brun, R. J.; Stofan, Andrew J.; and Berns, James A.: Management of Cryogenic Propellants in a Full-Scale Orbiting Space Vehicle. NASA TN D-4571, 1968.

3. Salzman, Jack A.; and Masica, William J.: Experimental Investigation of Liquid-Propellant Reorientation. NASA TN D-3789, 1967.

4. Sterbentz, W. H.: Liquid Propellant Thermal Conditioning System. Rep. LMSC-K-07-68-2, Lockheed Missiles & Space Co. (NASA CR-72365), Aug. 15, 1968.

5. Yang, Wen-Jei; Larsen, P. S.; and Clark, J. A.: Interfacial Heat and Mass Transfer in a Suddenly Pressurized Binary Liquid-Vapor System. J. Eng. Industry, vol. 87, no. 4, Nov. 1965, pp. 413-418.

6. Thomas, P. D.; and Morse, F. H.: Analytical Solution for the Phase Change in a Suddenly Pressurized Liquid-Vapor System. Advances in Cryogenic Engineering. Vol. 8. K. D. Timmerhaus, ed. Plenum Press, 1962, pp. 550-562.

7. Labus, Thomas L.; Aydelott, John C.; and Lacovic, Raymond F.: Low-Gravity Venting of Refrigerant 11. NASA TM X-2479, 1972.

8. Larkin, Bert K.; and Bowman, T. E.: The Venting of Saturated Liquids in Zero Gravity. Proceedings of the 13th Annual Technical Meeting of the Institute of Environmental Sciences. Vol. 2, 1967, pp. 591-598.

9. Anon.: Thermodynamic Properties of Refrigerants. American Society of Heating, Refrigerating, and Air-Conditioning Engineers, 1969.

10. Swalley, Frank E.; Ward, Wyley D.; and Toole, Louis E.: Low Gravity Fluid Behavior and Heat Transfer Results from the S-IV-B-203 Flight. Proceedings of the Conference on Long-Term Cryo-Propellant Storage in Space. NASA TM X-60666, 1966, pp. 213-232.

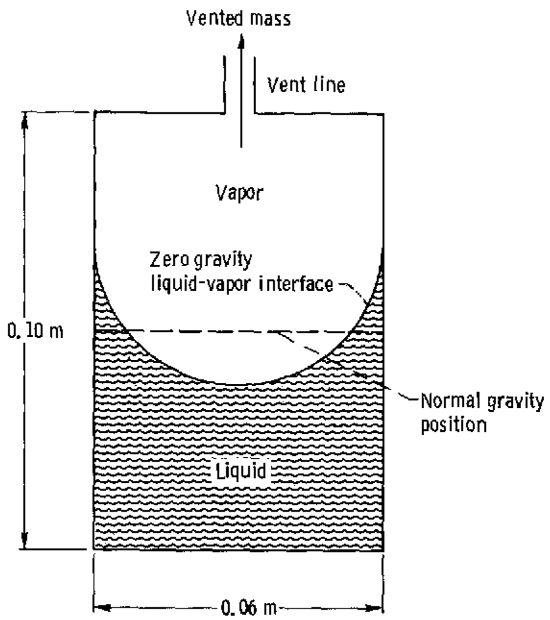

Figure 1. - Schematic drawing of typical test container showing interface position during zero gravity venting.

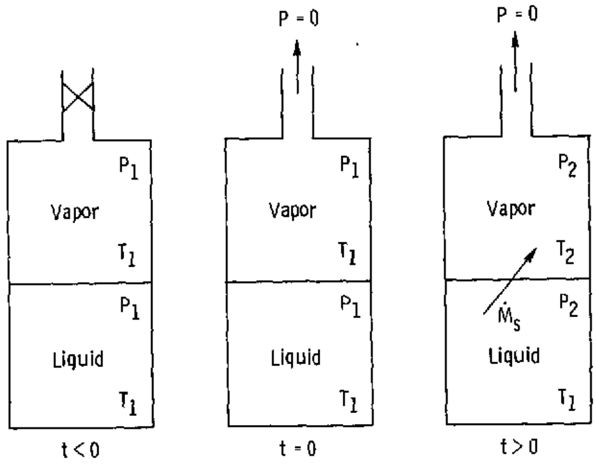

Figure 2. - Schematic drawing of interface mass transfer venting model.

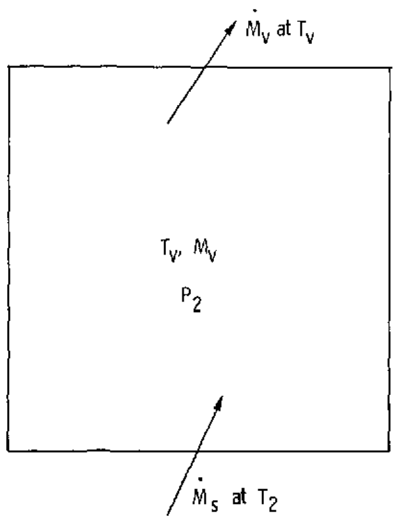

Figure 3. - Vapor region control volume.

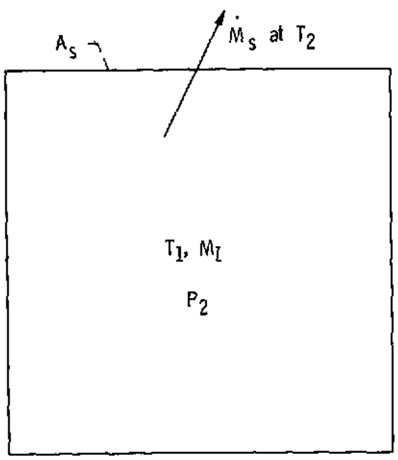

Figure 4. - Liquid region control volume.

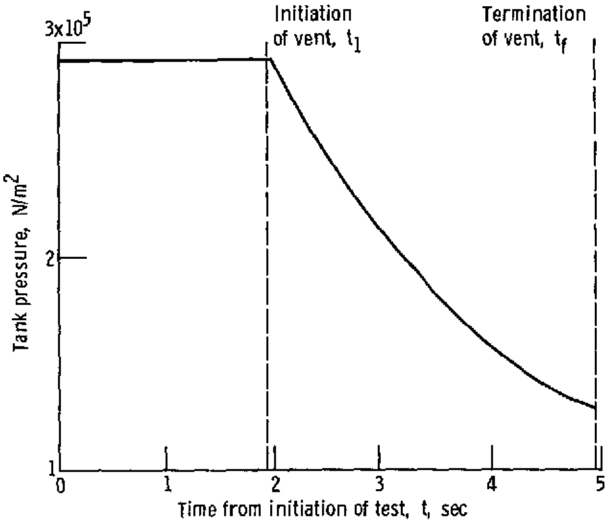

Figure 5. - Tank pressure response during representative data run. Test fluid, refrigerant C318; nozzle diameter, 0.132 centimeter; average vent rate, 0.5 ullage volume per second.

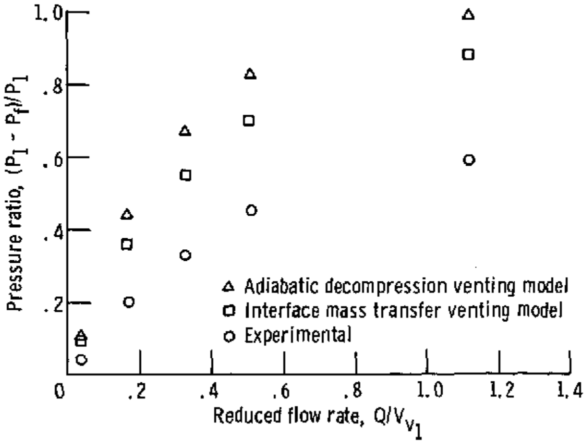

Figure 6. - Effect of volumetric flow rate on pressure drop for refrigerant 11.

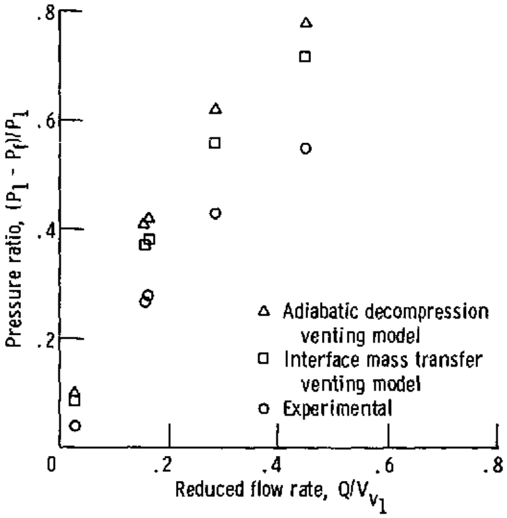

Figure 7. - Effect of volumetric flow rate on pressure drop for refrigerant C318.

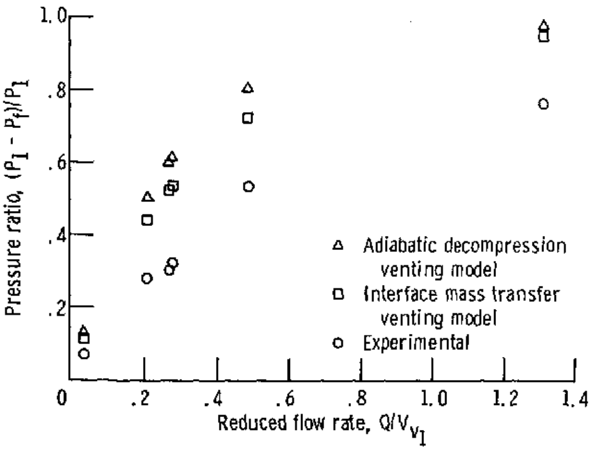

Figure 8. - Effect of volumetric flow rate on pressure drop for refrigerant 600.

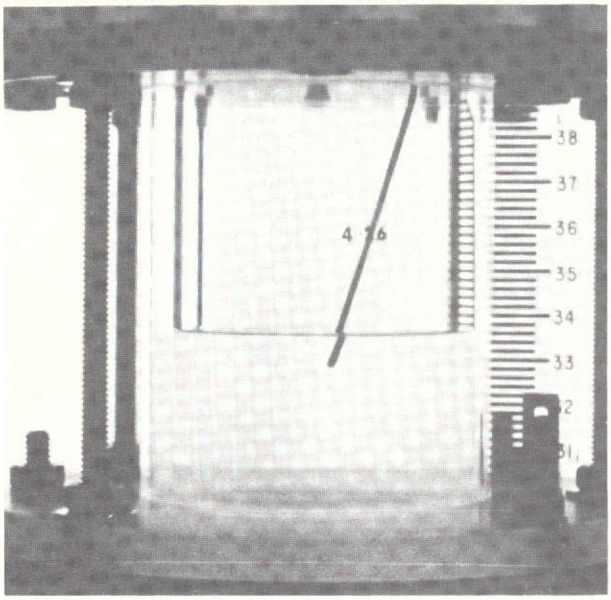

(a) Normal gravity initial condition. Time from initiation of test, 0 second.

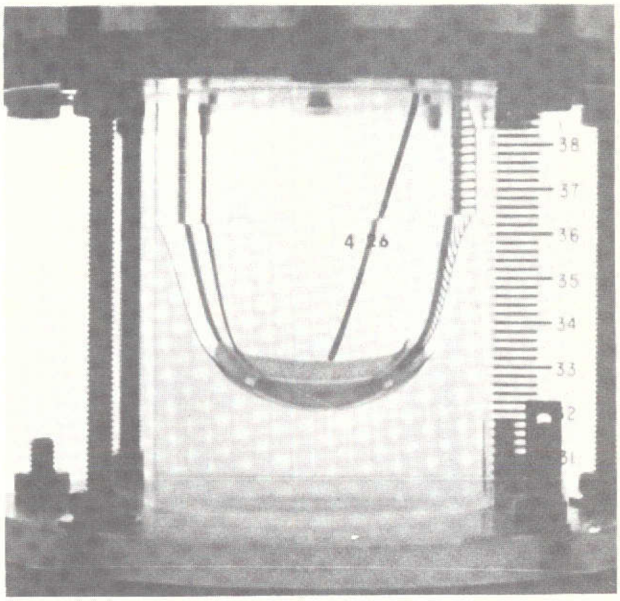

(b) Formation of zero-gravity equilibrium interface. Venting begins, time from initiation of test, 1.90 seconds.

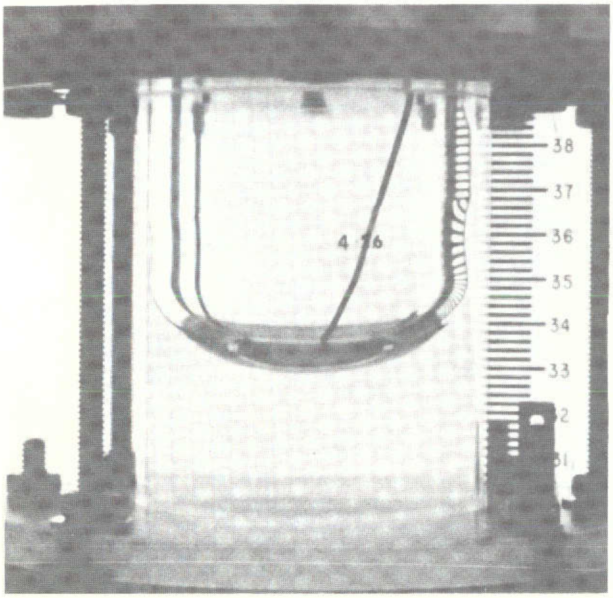

(c) Venting occurring. Time from initiation of test, 4.00 seconds.

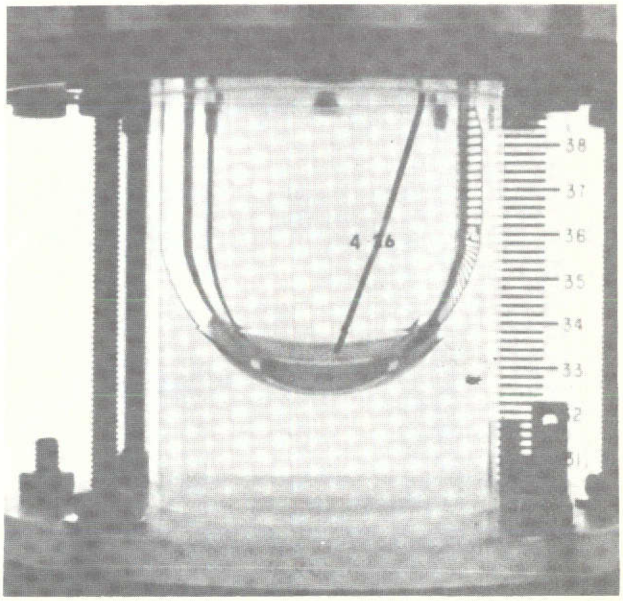

(d) Configuration prior to termination of test. No venting; time from initiation of test, 5.16 seconds.

Figure 9. - Typical test in which no bulk boiling occurs. Test fluid, refrigerant C318; nozzle diameter, 0.132 centimeter; inital ullage pressure, 2.90×10^5 newtons per square meter; average vent rate, 0.5 ullage volume per second.

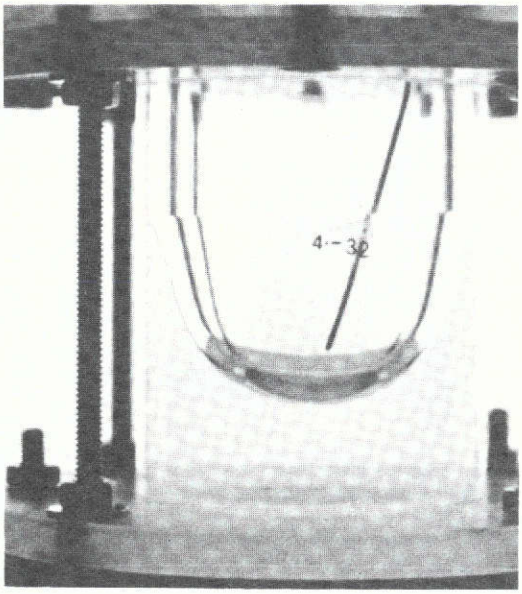

(a) Formation of zero-gravity equilibrium interface. Venting begins; time from initiation of test, 1.90 seconds.

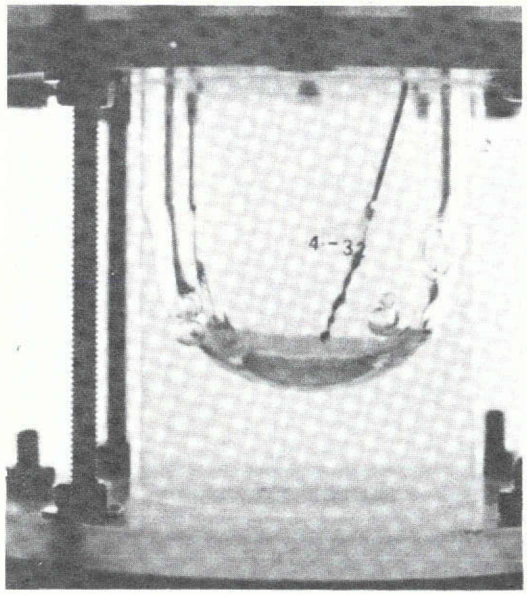

(b) Boiling occurs near liquid-vapor interface. Time from initiation of test, 2.70 seconds.

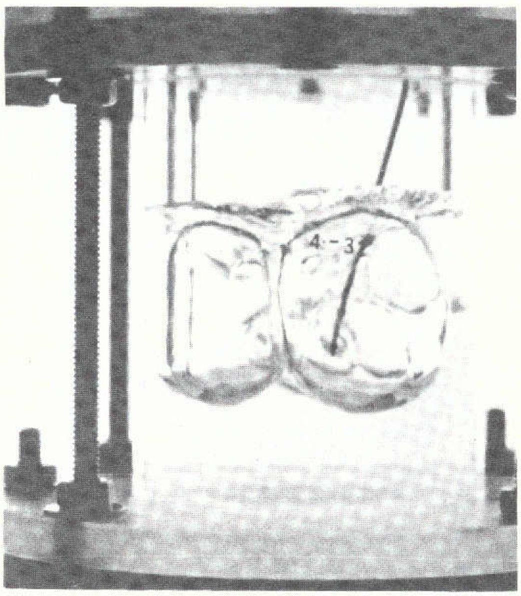

(c) Vapor generation increases; interface rise toward vent. Time from initiation of test, 4.00 seconds.

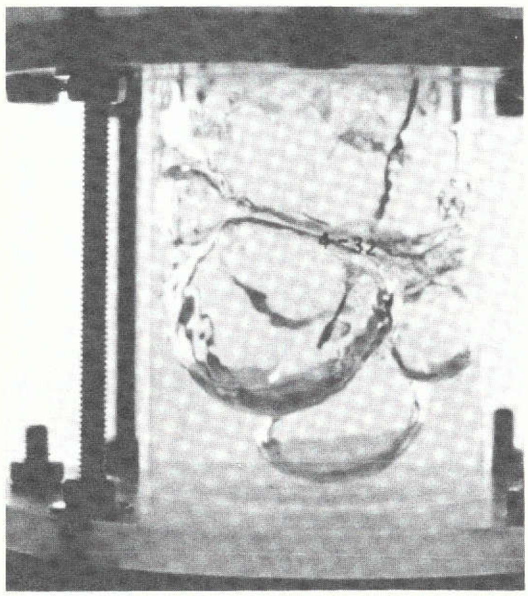

(d) Configuration prior to termination of test. No venting occurring; time from initiation of test, 5.17 seconds.

Figure 10. - Occurrence of bulk boiling in zero-gravity. Test fluid, refrigerant C318, nozzle diameter, 0.193 centimeter; initial ullage pressure, 2.76×10^5 newtons per square meter; average vent rate, 1.0 ullage volume per second.

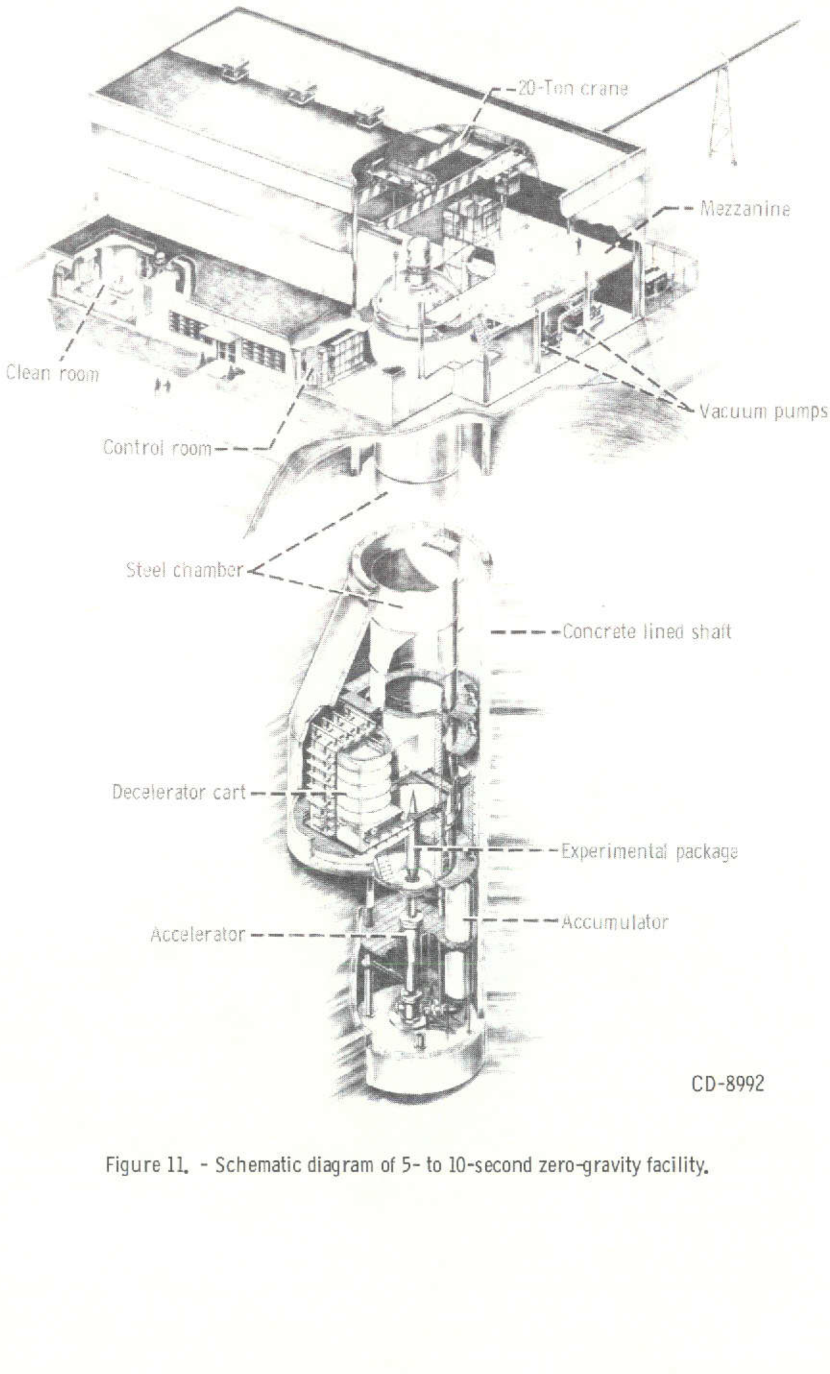

Figure 11. - Schematic diagram of 5- to 10-second zero-gravity facility.

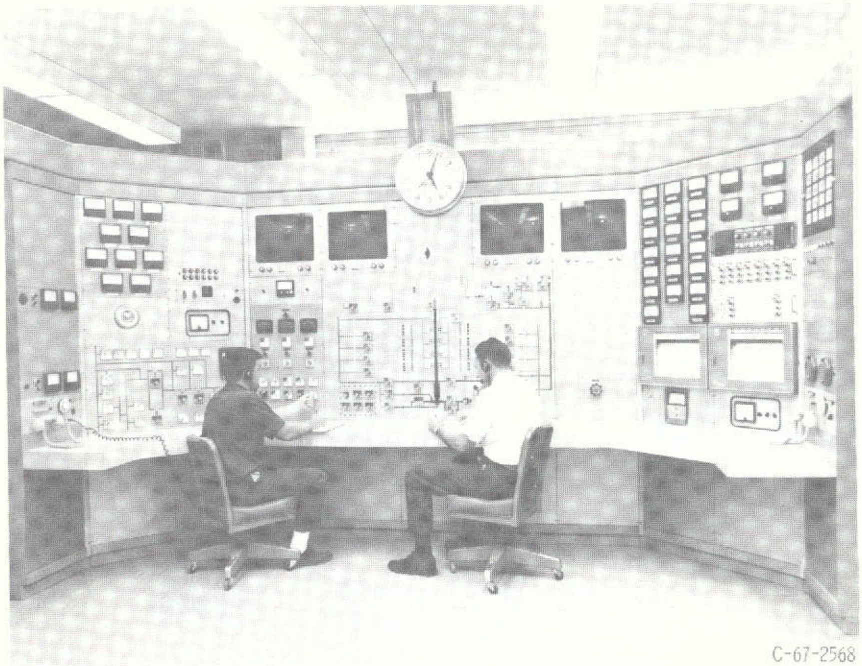

Figure 12. - Control room.

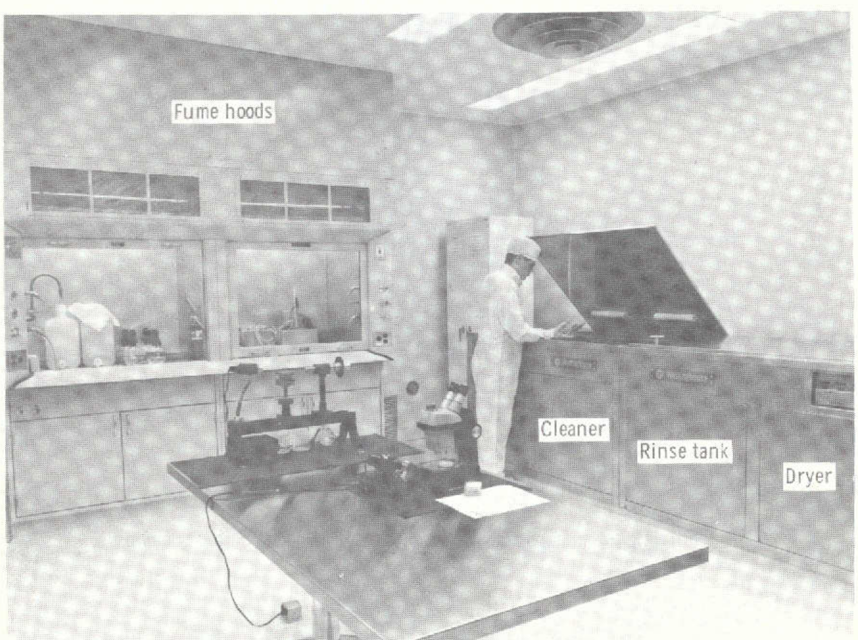

(a) Ultrasonic cleaning system.

Figure 13. - Facility clean room.

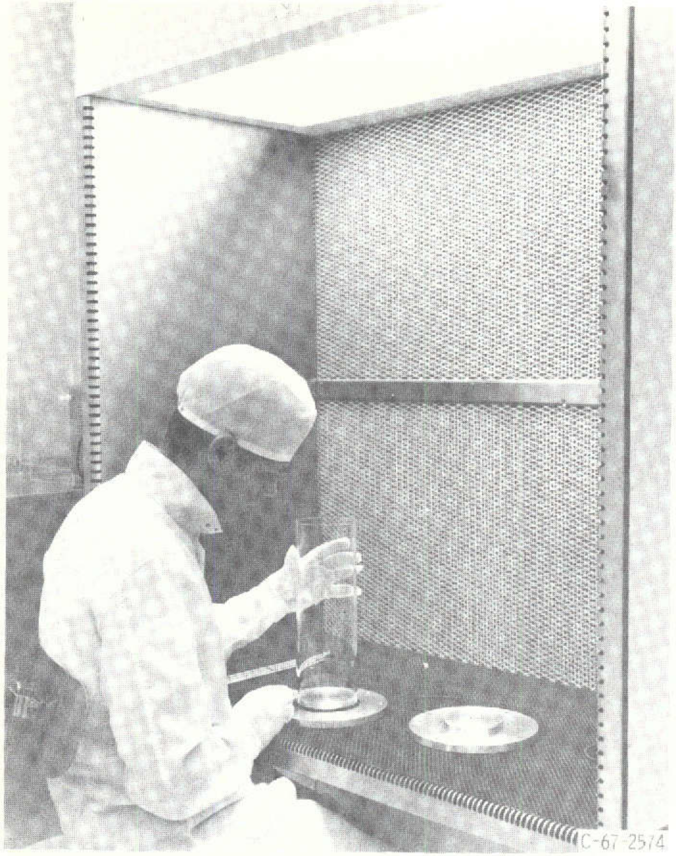

(b) Laminar flow work station.

Figure 13. - Concluded.

Figure 14. - Deceleration system.

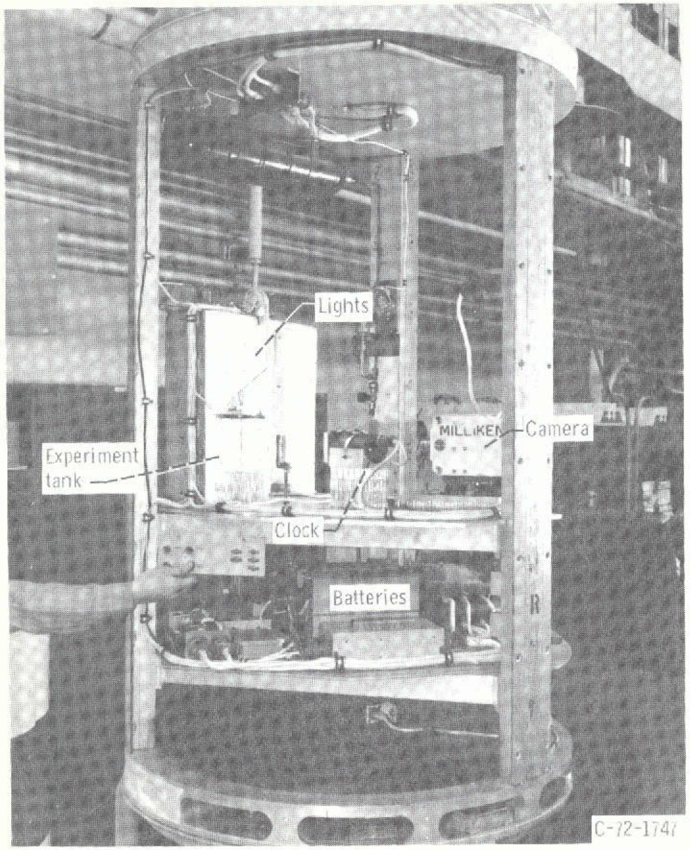

Figure 15. - Experiment vehicle.

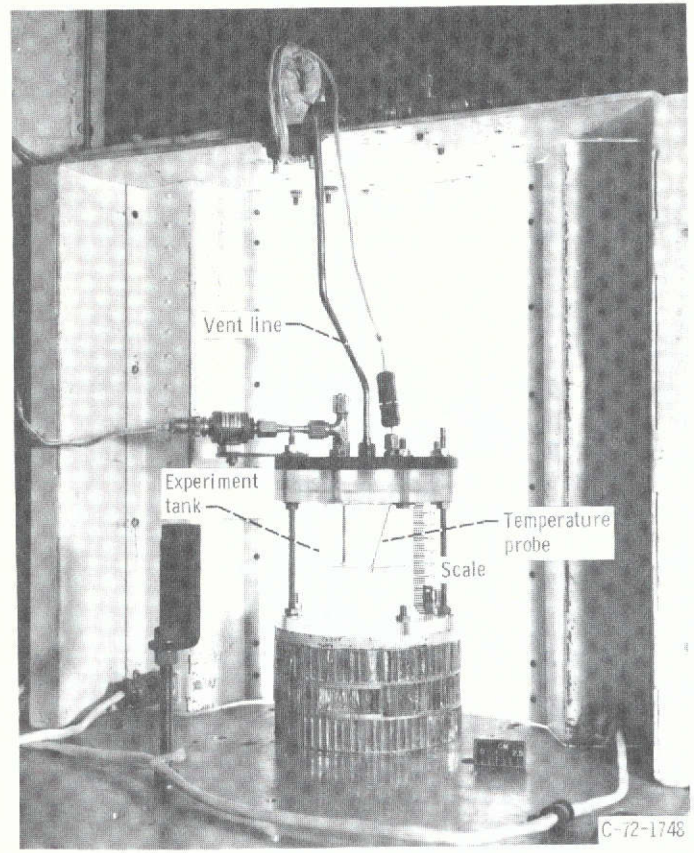

Figure 16. - Experiment assembly tray.

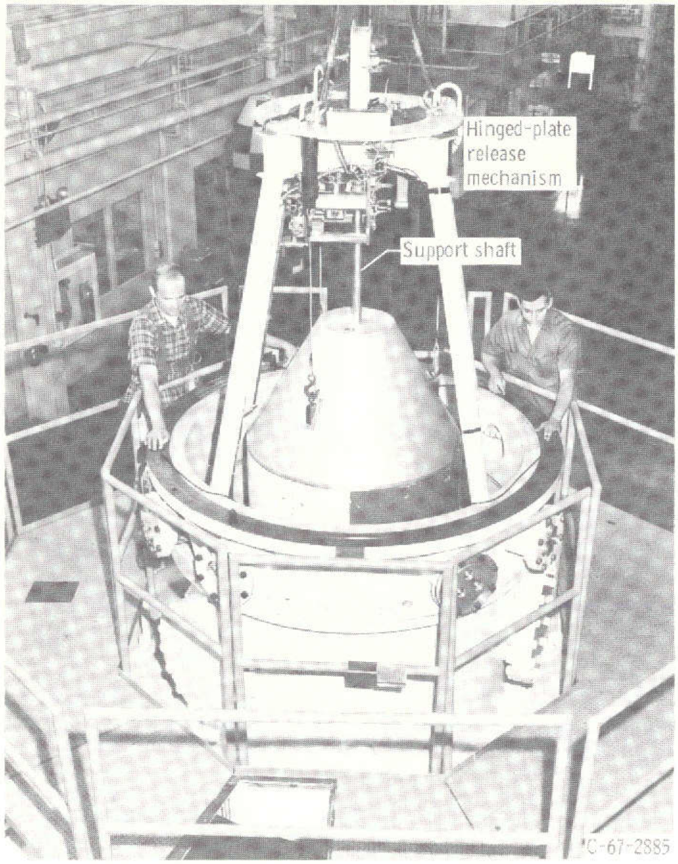

Figure 17. - Vehicle position prior to release.

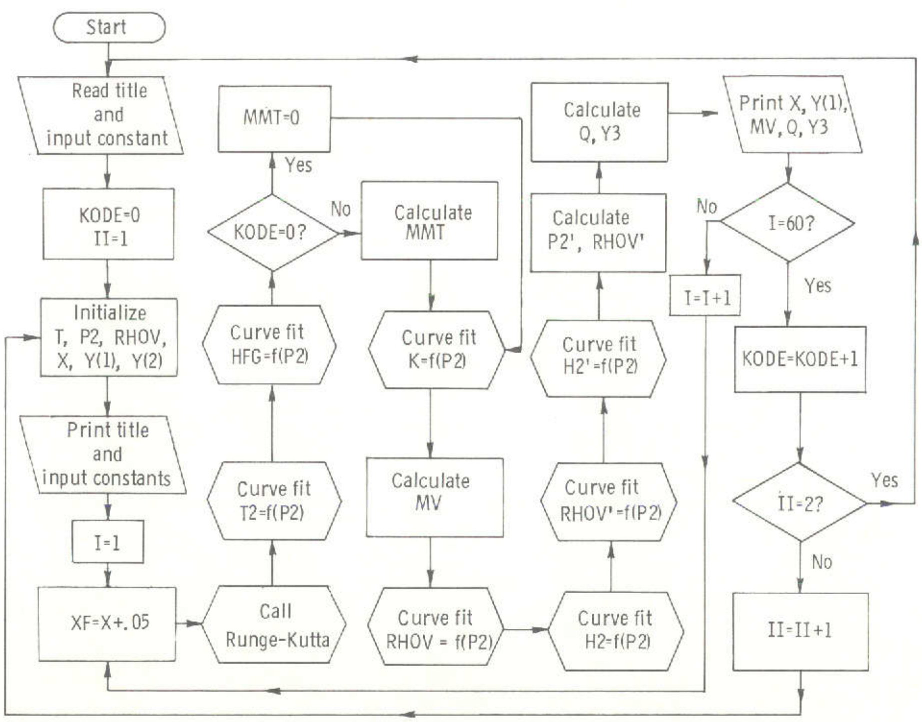

Figure 18. - Computer program flow chart.